EARTHQUAKE ENGINEERING AND STRUCTURAL DYNAMICS
Earthquake Engng Struct. Dyn. 2006; **35**:921–942
Published online 10 February 2006 in Wiley InterScience (www.interscience.wiley.com). DOI: 10.1002/eqe.559

Smart base isolated buildings with variable friction systems: H_∞ controller and SAIVF device

S. Narasimhan[1,2] and S. Nagarajaiah[3,*,†,‡]

[1]*Department of Civil and Environmental Engineering, Rice University, Houston, TX 77005, U.S.A.*
[2]*ABSG Consulting, Houston, Texas 77060, U.S.A.*
[3]*Department of Civil and Environmental Engineering and Mechanical Engineering and Material Science, Rice University, Houston, TX 77005, U.S.A*

SUMMARY

A new control algorithm is developed for reducing the response of smart base isolated buildings with variable friction semiactive control systems in near-fault earthquakes. The central idea of the control algorithm is to design a H_∞ controller for the structural system and use this controller to determine the optimum control force in the semiactive device. The H_∞ controller is designed using appropriate input and output weighting filters that have been developed for optimal performance in reducing near-fault earthquake responses. A novel semiactive variable friction device is also developed and with the H_∞ controller shown to be effective in achieving response reductions in smart base isolated buildings in near-fault earthquakes. The new variable friction device developed consists of four friction elements and four restoring spring elements arranged in a rhombus configuration with each arm consisting of a friction–stiffness pair. The level of friction force can be adjusted by varying the angle of the arms of the device leading to smooth variation of friction force in the device. Experimental results are presented to verify the proposed analytical model of the device. The H_∞ algorithm is implemented analytically on a five storey smart base isolated building with linear elastomeric isolation bearings and variable friction system located at the isolation level. The H_∞ controller along with the weighting filters leads to the smooth variation of friction force, thus eliminating the disadvantages associated with rapid switching. Several recent near-fault earthquakes are considered in this study. The robustness of the H_∞ controller is shown by considering a stiffness uncertainty of $\pm 10\%$. Copyright © 2006 John Wiley & Sons, Ltd.

KEY WORDS: H_∞; robust control; smart base isolated buildings; variable friction device; semiactive structural control; near-fault earthquakes

*Correspondence to: S. Nagarajaiah, Department of Civil and Environmental Engineering and Mechanical Engineering and Material Science, Rice University, Houston, TX 77005, U.S.A.
†E-mail: nagaraja@rice.edu
‡Associate Professor.

Contract/grant sponsor: National Science Foundation; contract/grant number: NSF-CAREER-CMS 9996290

Received 16 May 2005
Revised 14 November 2005
Accepted 14 November 2005

1. INTRODUCTION

Active and semiactive structural control has been studied extensively for the past two decades [1–4]. Active systems have large power requirements and may not be a practical for structures subjected to near-fault earthquakes. Semiactive systems require nominal power and provide a robust alternative to active systems. The application of semiactive systems such as variable stiffness, damping, and friction devices have been investigated and demonstrated to be effective by many researchers [5–18]. Semiactive control strategies using variable damping, and variable friction devices have been implemented on base isolated buildings [19–21] for reducing base displacements and superstructure responses [8, 22–26]. Most of the semiactive friction control algorithms and devices studied so far are on–off type and may result in increased structural shear.

Clipped optimal control of smart base isolated structures using H_2/LQG methods with variable damping devices has been studied extensively [24, 26, 27]. Clipped optimal control involves setting the level of semiactive damping force to either maximum or minimum based on the desired active force generated by the H_2/LQG controller. Lyapunov based controllers [28, 29], sliding mode controller [30], and absolute acceleration feedback controller [13] have been developed for smart base isolated structures. Robust control methods using H_∞ have also been studied [25, 31–34]. There have been no studies which apply H_∞ to semiactive control of smart base isolated buildings using friction devices. The semiactive friction devices studied so far vary the normal force across friction interfaces using either physical or electromagnetic means [6–8]. The level of normal force required is determined either by using structural responses directly such as prior peak displacement [10], or through other criteria derived based on Lyapunov methods [5] or using optimal controllers [6, 35]. The control algorithms developed in the aforementioned studies result in on–off switching laws. Although such algorithms are effective in reducing base displacements, in some cases the floor accelerations and the inter-storey drifts increase as a result of abrupt switching.

In this study, (i) a new semiactive independently variable friction (SAIVF) device capable of varying the level of friction smoothly is developed, and (ii) a new robust control algorithm based on H_∞ is developed to achieve response reductions in smart base isolated buildings subjected to a variety of near-fault earthquakes. The H_∞ controller is designed using appropriate input and output frequency dependent weighting filters that have been developed for smooth variation of friction force and for optimal performance in reducing near-fault earthquake responses. The effectiveness of the control algorithm in the presence of a structural stiffness uncertainty of $\pm 10\%$ is also presented.

2. STRUCTURE WITH VARIABLE FRICTION SYSTEM: FORMULATION

The state-space equations for the six degrees of freedom smart base isolated planar structure used in earlier studies [8] and shown in Figure 1 is as follows:

$$\dot{\mathbf{x}}(t) = \mathbf{A}\mathbf{x}(t) + \mathbf{B}u(t) + \mathbf{E}\ddot{u}_g(t) \tag{1}$$

where $\mathbf{x}$ consists of the states, $u(t) = f_d(t)$ is the control force from the SAIVF device, $\ddot{u}_g(t)$ is the foundation acceleration and $\mathbf{A}$, $\mathbf{B}$ and $\mathbf{E}$ are system matrices that are defined

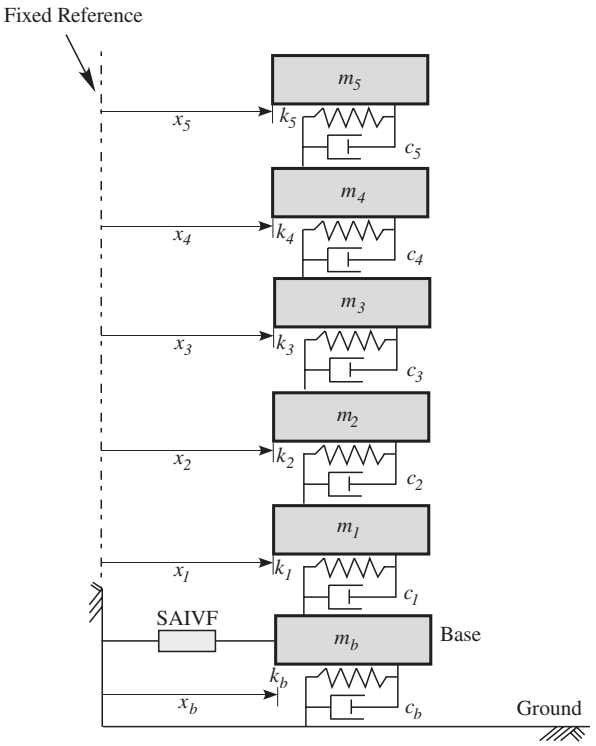

Figure 1. Five storey building model.

as follows:

$$\mathbf{A} = \begin{bmatrix} \mathbf{0} & \mathbf{I} \\ -\mathbf{M}^{-1}\mathbf{K} & -\mathbf{M}^{-1}\mathbf{C} \end{bmatrix}, \quad \mathbf{B} = \begin{bmatrix} \mathbf{0} \\ \mathbf{M}^{-1}\boldsymbol{\Lambda} \end{bmatrix}, \quad \mathbf{E} = -\begin{bmatrix} \mathbf{0} \\ \boldsymbol{\Gamma} \end{bmatrix}$$

In the above equations, $\mathbf{M}$ is a diagonal mass matrix formed using 6800 kg for the mass of the base and 5897 kg for the remaining five floors. The damping coefficients for the base and the five storeys are 7480, 67 000, 58 000, 57 000, 50 000 and 38 000 N s/m, respectively. The stiffness of the base is 231.5 kN/m and the stiffness of the five storeys are 33 732, 29 093, 28 621, 24 954 and 19 059 kN/m, respectively. The device location vector and the earthquake influence vectors are $\Lambda = [1\ 0\ 0\ 0\ 0\ 0]^{\mathrm{T}}$ and $\Gamma = [1\ 1\ 1\ 1\ 1\ 1]^{\mathrm{T}}$. The natural frequencies of the structure (without the SAIVF device) are 0.40, 5.46, 10.27, 14.67, 18.3 and 21.3 Hz respectively. The damping in the isolation system (without the SAIVF device) is so chosen to provide a damping ratio of 4% in the isolated case. The earthquakes used in this study are Newhall (1994 Northridge Earthquake, Newhall county, Fault-Normal 360 and Fault-Parallel 90), Sylmar (1994 Northridge Earthquake, Sylmar station, Fault-Normal 360 degrees and Fault-Parallel 90 degrees), Rinaldi (1994 Northridge Earthquake, Rinaldi station, Fault-Normal 228 degrees and Fault-Parallel 318 degrees), Kobe (1995, JMA station, East-West and North-South components), Jiji (1999, station TCU 068, East–West and

North–South components) and Erzikan (1992, 1719, Turkey, East–West and North–South components).

3. SEMIACTIVE VARIABLE FRICTION DEVICE (SAIVF)

The SAIVF device is based on the semiactive variable stiffness device (SAIVS) [12, 36]. The SAIVF device consists of four friction elements and four spring elements, each friction–stiffness pair in parallel, arranged in a rhombus configuration as shown in Figure 2. The spring–friction elements are connected to joints 1–4 as shown in Figure 2. Joint 1 is fixed in the x direction and can be positioned in the y direction by a linear electromechanical actuator and controller. Joint 2 is free to move in both the x and y directions. Joints 3 and 4 are free to move only in the x direction. The ends of the guide rail, on which joint 2 moves, are attached to the base slab. The ends of the guide rail, on which joints 3 and 4 move are attached to the foundation. The electromechanical actuator is fixed to the foundation and can actuate in the y direction thus moving joint 1 to the required position. Each of the pair of elements are located at an angle, θ to the horizontal. The stiffness elements act as restoring devices and their contribution to the overall system stiffness (stiffness of the elastomeric isolation system) is minimum. The SAIVF device is capable of providing smooth variation of the level of

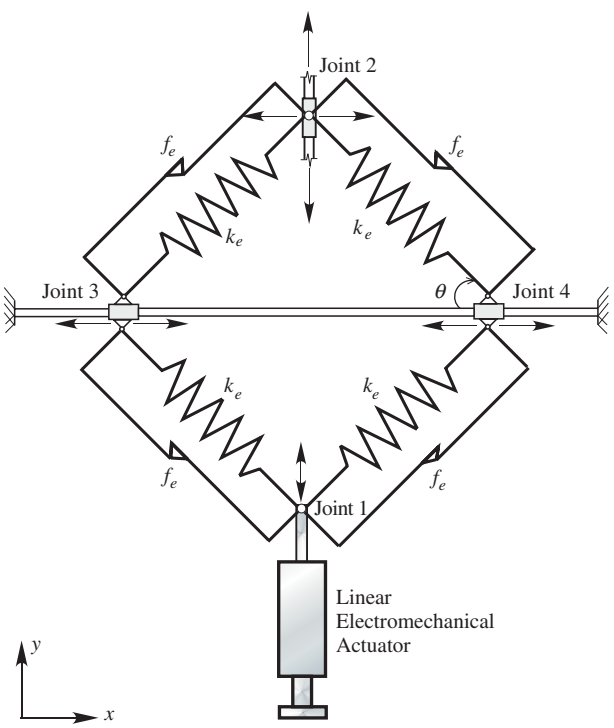

Figure 2. Analytical model of the variable friction device.

friction force by varying the angle (θ) of the arms of the device (a spring–friction element pair) using the linear electromechanical actuator to position the joint 1 appropriately. The magnitude of force developed in the device is a function of the angle, θ, given by

$$f_d(t) = k_e f(\theta,t)^2 y_d(t) + c_e z f(\theta,t) \tag{2}$$

where, $y_d(t)$ is the displacement in the x direction at joint 2, k_e is the stiffness of single spring, $\theta(t)$ is the time varying angle of the spring elements with the horizontal, $f_e = c_e z$, c_e is a constant and z is the friction parameter [37, 38] obtained by solving the following differential equation:

$$Y\dot{z} + \gamma|\dot{y}_d|z|z| + \beta\dot{y}_d z^2 - \dot{y}_d = 0 \tag{3}$$

where $\dot{y}_d$ is the velocity at the joint 2, Y is the yield displacement of the friction element, γ and β are constants.

The angle, θ can only vary between angles 0 and $\pi/2$. The time-varying function $f(\theta,t)$ is the cosine of angle θ and given as

$$f(\theta,t) = \cos\,\theta(t)[0 \leqslant \theta \leqslant \pi/2] \tag{4}$$

4. EXPERIMENTAL STUDY AND VERIFICATION

In order to verify the analytical model of the semiactive device proposed in Equation (2), experimental studies were conducted on a small-scale model of the device. The experiments consisted of recording the force developed in the device while excited by a 0.5 Hz sinusoid. The magnitude of the force in the device for two positions, $\theta = 10^\circ$ (closed), and $\theta = 77^\circ$ (open), are shown in Figure 3. The angle, θ is calculated based on the device position at joint 1 (Figure 2). The response of the device to real-time switching is also shown at $t = 8$ s, when the device is switched from closed to open positions while excited by the sinusoid. Figure 4 shows the comparison of experimental and simulated force–displacement relationship for the variable friction device. Equation (2) is used to simulate the force corresponding to the device positions measured in the experiment as shown in Figure 3. The parameters of the analytical model were determined by a least-squares fit of the experimental data. The comparison study shows that the analytical model for the device provides a satisfactory representation of the force in the SAIVF device for both open and closed positions; however, the analytical model does not simulate the behaviour of the device accurately in all regions.

To demonstrate the smooth variation of friction, the force–displacement loops of the full-scale SAIVF device (to be used in the numerical example) is simulated using the analytical model for various values of θ and shown Figure 5. The force generated by the device is due to a sinusoidal excitation with frequency, $\omega = 2\pi$ rad/s and amplitude of 1 m.

5. CONTROL DESIGN IN THE FREQUENCY DOMAIN AND H_∞ FORMULATION

Frequency domain control methods such as H_∞ [39] provide the necessary framework to introduce frequency-shaping filters in the control design. Such filters enable the designer to better inform the controller about the input excitation and desired output response frequency

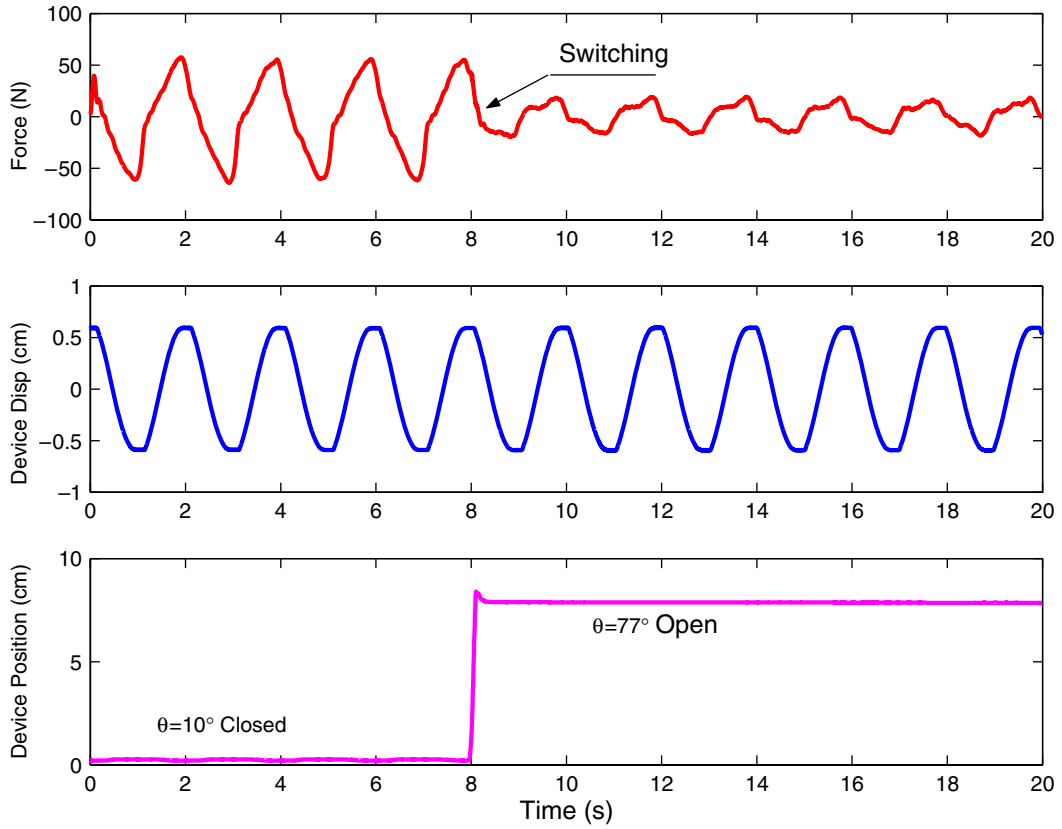

Figure 3. Experimental results—force developed in the SAIVF device excited by a 0.5 Hz, sinusoid with an amplitude of 0.25 in for two values of θ.

characteristics. The input excitation filter is obtained by appending two second-order filters in series. The first filter is obtained by a least-squares fit of earthquake data and closely models the power spectral density of the foundation excitation for a set of chosen near-fault earthquakes and has been used by the authors in the benchmark study on base isolated buildings [27]. This input excitation filter is represented in the frequency domain as follows:

$$F(s) = \frac{4\zeta_g \omega_g s}{s^2 + 2\zeta_g \omega_g s + \omega_g^2}, \quad \text{where } \omega_g = 2\pi \text{ rad/s}, \quad \zeta_g = 0.3 \tag{5}$$

Appending another second-order filter having a transfer function, $(2\zeta_g\omega_g s)/[s^2+2\zeta_g\omega_g s+\omega_g^2]$ to the filter in Equation (5), results in a higher order filter. The filters (the two second-order filters and the higher order filter obtained by appending the two filters in series) and the spectral densities of selected earthquakes are shown in Figure 6. The filter so obtained accentuates the energy content of the earthquake in the 1 Hz frequency range and drops off sharply on either side of this central frequency, resulting in an improved controller performance and

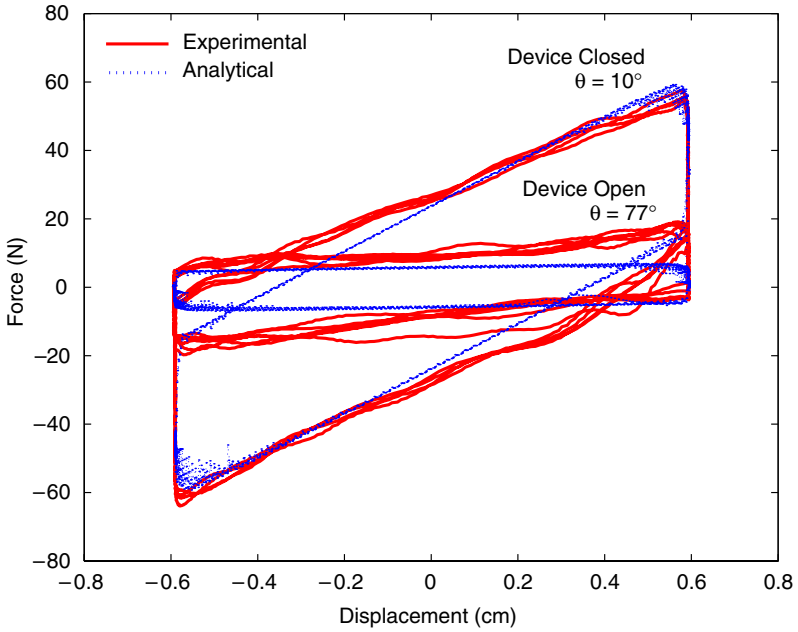

Figure 4. Comparison of experimental and analytical force–displacement loops of the small scale SAIVF device for two values of θ.

can be written as

$$F(s) = \frac{8\zeta_g^2\omega_g^2 s^2}{[s^2 + 2\zeta_g\omega_g s + \omega_g^2]^2} \tag{6}$$

where $\omega_g = 2\pi$ rad/s and $\zeta_g = 0.3$. The outputs are weighted using a first-order filter of the form, $W = a/(s + a)$, where $a = 3.5$ rad/s, which determines the roll-off frequency. A first-order filter is used for output weighting as the control objective is to regulate the fundamental mode responses of the structure.

The input excitation filter [27] can be written in the state-space form as

$$\dot{\mathbf{x}}_f = \mathbf{A}_f\mathbf{x}_f + \mathbf{B}_f w$$

$$\ddot{U}_g = \mathbf{C}_f\mathbf{x}_f \tag{7}$$

where w is the white noise excitation, $\mathbf{x}_f$ are the states of the input filter, and the system matrices for the filter are given by,

$$A_f = \begin{bmatrix} 0 & 1 & 0 & 0 \\ 0 & 0 & 1 & 0 \\ 0 & 0 & 0 & 1 \\ -\omega_g^4 & -4\varsigma_g\omega_g^3 & -4\varsigma_g^2\omega_g^2 - 2\omega_g^2 & -2\varsigma_g\omega_g \end{bmatrix}, \quad \mathbf{B}_f = [0 \quad 0 \quad 0 \quad 1]^{\mathrm{T}}$$

$$C_f = [0 \quad 0 \quad 8\varsigma_g^2\omega_g^2 \quad 0]$$

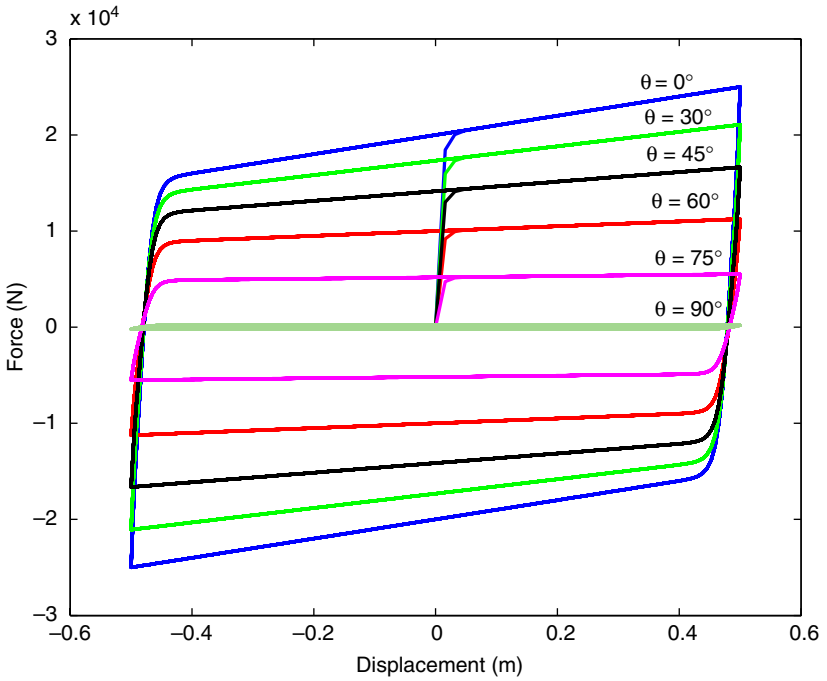

Figure 5. Force generated in the full-scale SAIVF device due to sine excitation of $\omega = 2\pi$ rad/s for various values of θ.

Similarly, the output weighting filter is written in the state-space form as

$$\dot{\mathbf{x}}_o = \mathbf{A}_o\mathbf{x}_o + \mathbf{B}_o\mathbf{x} \tag{8}$$

$$\mathbf{z}_o = \mathbf{C}_o\mathbf{x}_o \tag{9}$$

where $\mathbf{x}_o$ are the states of the output filter, $\mathbf{A}_o$, $\mathbf{B}_o$, and $\mathbf{C}_o$ are the system matrices. Augmenting the state equations in Equation (1) with the input excitation and output filter, the resulting state equation becomes,

$$\begin{bmatrix} \dot{\mathbf{x}} \\ \dot{\mathbf{x}}_f \\ \dot{\mathbf{x}}_o \end{bmatrix} = \begin{bmatrix} \mathbf{A} & \mathbf{E}\mathbf{C}_f & \mathbf{0} \\ \mathbf{0} & \mathbf{A}_f & \mathbf{0} \\ \mathbf{B}_o & \mathbf{0} & \mathbf{A}_o \end{bmatrix} \begin{Bmatrix} \mathbf{x} \\ \mathbf{x}_f \\ \mathbf{x}_o \end{Bmatrix} + \begin{bmatrix} \mathbf{0} \\ \mathbf{B}_f \\ \mathbf{0} \end{bmatrix} w + \begin{bmatrix} \mathbf{B} \\ \mathbf{0} \\ \mathbf{0} \end{bmatrix} u \tag{10}$$

The H_∞ control design is based on the linear system described in Equation (1). In the control formulation, the regulated outputs contains the base displacement, inter-storey drifts and the total accelerations of all floors, written as $[\mathbf{x}_b, \mathbf{x}_i - \mathbf{x}_{i-1}, \ddot{\mathbf{x}}_b, \ddot{\mathbf{x}}_i]$, where i corresponds to the floor number, $1, 2, \ldots, 5$. The measured outputs for the H_∞ controller contains the foundation acceleration, the base acceleration, and total accelerations of all floors, written as $[\ddot{U}_g, \ddot{\mathbf{x}}_b, \ddot{\mathbf{x}}_i]$, where i corresponds to the floor number. The external disturbance, $w = \ddot{U}_g$ is

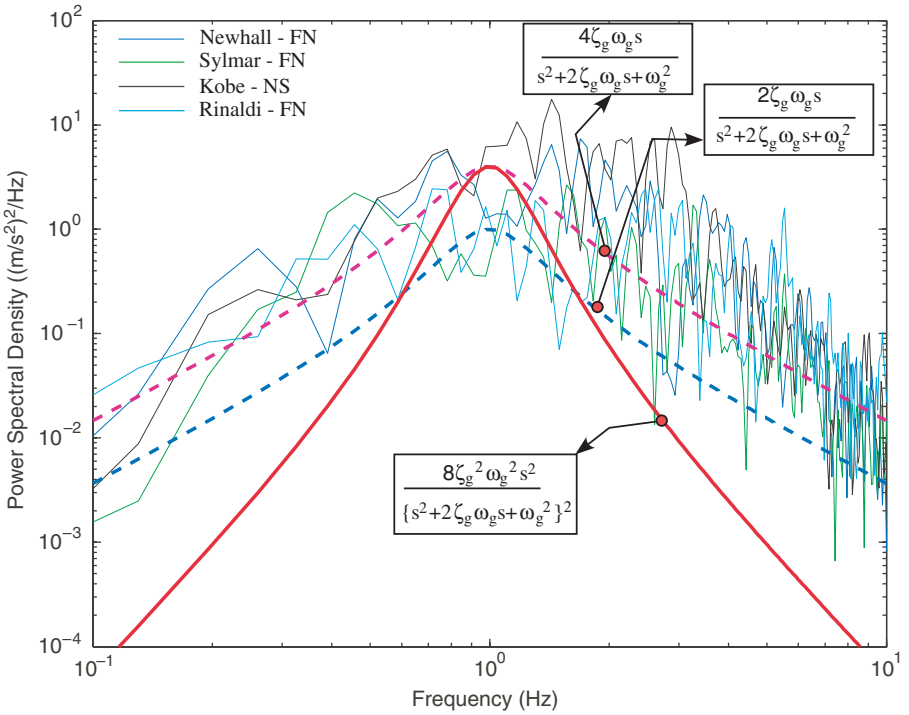

Figure 6. Excitation filter and power spectral density of earthquakes.

augmented to contain both the external disturbance and the measurement noise and is contained in the vector, $\mathbf{w} = [\ddot{U}_g, \mathbf{v}]^T$, where $\mathbf{v}$ is the measurement noise. Additionally, the device displacement, y_d, is also measured for the control algorithm. However, this measurement is not used in the H_∞ controller formulation. The augmented state-space equations can now be written as

$$\dot{\mathbf{x}}_\mathbf{a} = \mathbf{A}\mathbf{x}_\mathbf{a} + \mathbf{B_1}\mathbf{w} + \mathbf{B_2}u \tag{11}$$

$$\mathbf{z} = \mathbf{C_1}\mathbf{x}_\mathbf{a} + \mathbf{D_{11}}\mathbf{w} + \mathbf{D_{12}}u \tag{12}$$

$$\mathbf{y} = \mathbf{C_2}\mathbf{x}_\mathbf{a} + \mathbf{D_{21}}\mathbf{w} + \mathbf{D_{22}}u \tag{13}$$

where, $\mathbf{z}$ are the regulated outputs, $\mathbf{y}$ are the measurements, $\mathbf{x}_a = [\mathbf{x}\ \ \dot{\mathbf{x}}_f\ \ \dot{\mathbf{x}}_o]^T$, $\mathbf{B_1} = [\mathbf{0}\ \ \mathbf{B}_f\ \ \mathbf{0}]^T$, $\mathbf{B_2} = [\mathbf{B}\ \ \mathbf{0}\ \ \mathbf{0}]^T$ and $\mathbf{C}_1$, $\mathbf{C}_2$, $\mathbf{D}_{11}$, $\mathbf{D}_{12}$, $\mathbf{D}_{21}$, $\mathbf{D}_{22}$ are mapping matrices of appropriate dimensions.

The basic block diagram [40] is shown in Figure 7. The generalized plant is represented by G and the controller by K. The measurement outputs are represented by y, the outputs to be regulated by z, external disturbance by w, which includes the earthquake excitation and sensor noise and the control input is represented by u. The purpose of the H_∞ control method is to minimize the ∞-norm of the transfer function from input $\mathbf{w}$ to regulated output $\mathbf{z}$, $\mathbf{G}_{zw}$

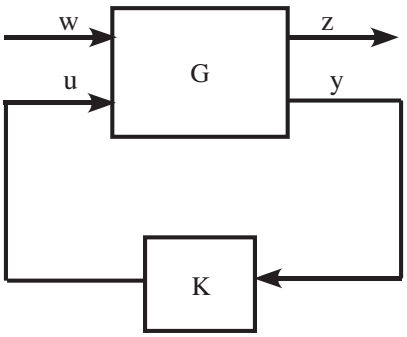

Figure 7. Basic block diagram for control design.

and is written as

$$\|\mathbf{G_{zw}}(s)\|_\infty = \sup_\omega[\bar{\sigma}(\mathbf{G_{zw}}(s))] \leqslant \gamma \tag{14}$$

$\bar{\sigma}$ is the largest singular value of the transfer function, sup denotes the supremum and γ is a positive bound for the norm. The solution for the controller for the generalized regulator problem [41–43] is given by

$$u = -\mathbf{F}_\infty \hat{\mathbf{x}} \tag{15}$$

and the state estimator is given by

$$\dot{\hat{\mathbf{x}}} = \mathbf{A}\hat{\mathbf{x}} + \mathbf{B_2}u + \mathbf{B_1}\hat{\mathbf{w}} + \mathbf{J}_\infty \mathbf{L}_\infty(\mathbf{y} - \hat{\mathbf{y}}) \tag{16}$$

where

$$\hat{\mathbf{w}} = \gamma^{-2}\mathbf{B}_1'\mathbf{K}_\infty\hat{\mathbf{x}}$$

and

$$\hat{\mathbf{y}} = \gamma^{-2}\mathbf{D_{21}}\mathbf{B}_1'\mathbf{K}_\infty\hat{\mathbf{x}} + \mathbf{C_2}\hat{\mathbf{x}}$$

The term, $\hat{\mathbf{w}}$ and $\hat{\mathbf{y}}$ are the estimates of the worst-case disturbance and output of the estimator. There exists a stabilizing controller if and only if there exists positive semi-definite solutions to the two Riccatti equations for $\mathbf{K}_\infty$ and $\mathbf{N}_\infty$ and the condition

$$\rho(\mathbf{K}_\infty\mathbf{N}_\infty) < \gamma^2 \tag{17}$$

where $\rho(A)$ is the spectral radius of A which is defined as the largest singular value of A. The controller written in the packed matrix notation is

$$\mathbf{K}_{\text{sub}}(s) = \begin{bmatrix} \hat{\mathbf{A}}_\infty & \mathbf{J}_\infty\mathbf{L}_\infty \\ -\mathbf{F}_\infty & \mathbf{0} \end{bmatrix} \tag{18}$$

where

$$\mathbf{F}_\infty = (\mathbf{D}_{12}'\mathbf{D}_{12})^{-1}(\mathbf{B}_2'\mathbf{X}_\infty + \mathbf{D}_{12}'\mathbf{C}_1)$$

$$\mathbf{L}_\infty = (\mathbf{Y}_\infty\mathbf{C}_2' + \mathbf{B}_1\mathbf{D}_{21}')(\mathbf{D}_{21}\mathbf{D}_{12}')^{-1}$$

and

$$\mathbf{J}_\infty = (\mathbf{I} - \gamma^{-2}\mathbf{Y}_\infty\mathbf{X}_\infty)^{-1}$$

The terms, $\mathbf{K}_\infty$ and $\mathbf{N}_\infty$ are the solutions to the controller and estimator Riccati equations given by

$$\mathbf{K}_\infty = \mathrm{Ric}\begin{pmatrix} \mathbf{A} - \mathbf{B}_2\tilde{\mathbf{D}}_{12}\mathbf{D}_{12}'\mathbf{C}_1 & \gamma^{-2}\mathbf{B}_1\mathbf{B}_1' - \mathbf{B}_2\tilde{\mathbf{D}}_{12}\mathbf{B}_2' \\ \tilde{\mathbf{C}}_1'\tilde{\mathbf{C}}_1 & -(\mathbf{A} - \mathbf{B}_2\tilde{\mathbf{D}}_{12}\mathbf{D}_{12}'\mathbf{C}_1)' \end{pmatrix} \tag{19}$$

$$\mathbf{N}_\infty = \mathrm{Ric}\begin{pmatrix} (\mathbf{A} - \mathbf{B}_1\mathbf{D}_{21}\tilde{\mathbf{D}}_{21}\mathbf{C}_2)' & \gamma^{-2}\mathbf{C}_1'\mathbf{B}_1 - \mathbf{C}_2'\tilde{\mathbf{D}}_{21}\mathbf{C}_2 \\ -\tilde{\mathbf{B}}_1\tilde{\mathbf{B}}_1' & -(\mathbf{A} - \mathbf{B}_1\tilde{\mathbf{D}}_{21}'\tilde{\mathbf{D}}_{21}\mathbf{C}_2) \end{pmatrix} \tag{20}$$

where

$$\tilde{\mathbf{C}}_1 = (\mathbf{I} - \mathbf{D}_{12}\tilde{\mathbf{D}}_{12}\mathbf{D}_{12}')\mathbf{C}_1$$

$$\tilde{\mathbf{B}}_1 = \mathbf{B}_1(\mathbf{I} - \mathbf{D}_{21}'\tilde{\mathbf{D}}_{21}\mathbf{D}_{21})$$

$$\tilde{\mathbf{D}}_{12} = (\mathbf{D}_{12}'\mathbf{D}_{12})^{-1} \quad \tilde{\mathbf{D}}_{21} = (\mathbf{D}_{21}\mathbf{D}_{21}')^{-1}$$

6. CONTROL ALGORITHM

The device position is determined by equating the force in the SAIVF device, $f_d(t)$, to the optimal force generated by the H_∞ controller. The resulting equations for the unknown variable $f(\theta,t)$ can be written as

$$f_d(t) = k_e f(\theta,t)^2 y_d(t) + c_e z f(\theta,t) = -\mathbf{K}_\infty\hat{\mathbf{x}}_a = F_\infty \tag{21}$$

where $\hat{\mathbf{x}}_a$ are the estimated states. Solving the above equation for the device position, $f(\theta,t)$, results in the following:

$$f(\theta,t) = \frac{-c_e z \pm \sqrt{c_e^2 z^2 + 4 y_d F_\infty k_e}}{2k_e y_d} \tag{22}$$

Due to the physical characteristics of the SAIVF device, the value of $f(\theta,t)$ is positive and bounded between 0 and $+1$; θ is bounded between 0 and $\pi/2$ at these values of $f(\theta,t)$.

Since there are two roots for the quadratic expression in Equation (22), maximum value is chosen for the unknown variable and is written as

$$\hat{f}(\theta,t) = \max\left\{\frac{|-c_e z \pm \sqrt{c_e^2 z^2 + 4 y_d F_\infty k_e}|}{2k_e|y_d|}\right\} \tag{23}$$

In case $|y_d| < 0.01$ m, then $|y_d| = 0.01$ m is used in the algorithm in order to prevent numerical difficulties. The values obtained by Equation (23) is passed through a low-pass filter to alleviate the high frequency switching.

The control law can be written as

$$\hat{f}_c(\theta,t) = \begin{cases} 1 & (v > 1) \\ v & \\ 0 & (v < 0) \end{cases} \tag{24}$$

where v is the output of the first-order filter,

$$\dot{v} = -a_1 v + a_2 \hat{f}(\theta,t) \tag{25}$$

The force in the SAIVF device can now be estimated as

$$f_d(t) = k_e \hat{f}_c(\theta,t)^2 y_d(t) + c_e z \hat{f}_c(\theta,t) \tag{26}$$

The values of a_1 and a_2 in Equation (25) are assumed to be 10.0 rad/s. All the simulations are performed in Matlab/Simulink [44] as shown in Figure 8.

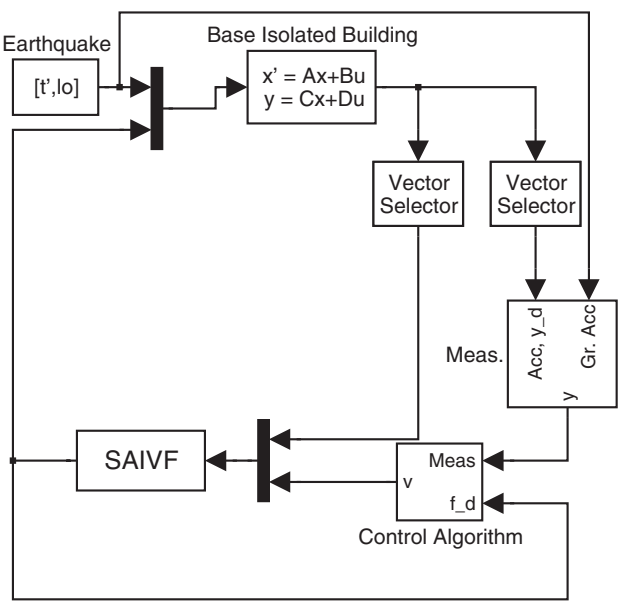

Figure 8. Matlab/Simulink control algorithm implementation.

7. RESULTS AND DISCUSSION

A set of nine performance indices, J1–J9 shown in Table I have been used to assess the performance of the control algorithm and SAIVF device. The indices J1–J5 measure the peak values of base shear, structural shear, base displacement, inter-storey drift and floor accelerations, respectively. These values are normalized by their respective uncontrolled values. In the following discussion, the term 'uncontrolled' refers to the case when there is no force feed back to the structure and the control device (active or semiactive) is disconnected from the structural system. The term 'passive' or 'closed' refers to the device when, $\theta = 0°$ (it is assumed in this study that it is possible to realize values close to $\theta = 0°$), where the device generates maximum force at all times. The performance index J6 measures the maximum control force developed in the device normalized by the peak base shear. The indices, J7 and J8 measure the RMS values of displacement and base acceleration normalized by their uncontrolled values. The index J9 measures the energy dissipated by the semiactive device as a percentage of the input excitation energy.

The H_∞ active and semiactive control algorithms are studied analytically with the base isolated building having no stiffness uncertainty. The results for the active control case are presented in Table II in terms of the performance indices described earlier and listed in Table I. The base and structural shears (base shear is at the isolation level and the structural shear is measured at all floors and the maximum value at the base of the first floor columns is chosen) in the case of active control are reduced between 18 and 38% in all cases except Jiji (where the semiactive passive case outperforms the active case) when compared to the passive case ($\theta = 0°$) and 10–57% when compared to the uncontrolled case. The reduction in base displacement is between 3 and 25% in a majority of earthquakes (except Jiji and Newhall-FP) when compared to the passive case and 19–62% when compared to the uncontrolled case. Reductions in the inter-storey drifts between 20 and 37 % are achieved in a majority of earthquakes (except Jiji) when compared to the passive case and 10–56% when compared to the

Table I. Performance indices.

Peak base shear*	Peak structure shear*	Peak base displacement*
$\mathrm{J1} = \dfrac{\max_t \lVert V_0(t) \rVert}{\max_t \lVert \hat{V}_0(t) \rVert}$	$\mathrm{J2} = \dfrac{\max_t \lVert V_1(t) \rVert}{\max_t \lVert \hat{V}_1(t) \rVert}$	$\mathrm{J3} = \dfrac{\max_t \lVert x_b(t) \rVert}{\max_t \lVert \hat{x_b}(t) \rVert}$
Peak interstorey drift*	Peak floor acceleration*	Peak control force
$\mathrm{J4} = \dfrac{\max_{t,f} \lVert d_f(t) \rVert}{\max_{t,f} \lVert \hat{d}_f(t) \rVert}$	$\mathrm{J5} = \dfrac{\max_{t,f} \lVert a_f(t) \rVert}{\max_{t,f} \lVert \hat{a}_f(t) \rVert}$	$\mathrm{J6} = \dfrac{\max_t \lVert f_d(t) \rVert}{\max_t \lVert V_0(t) \rVert}$
RMS base displacement*	RMS floor acceleration*	Energy dissipated by SAIVF
$\mathrm{J7} = \dfrac{\max_i \lVert \sigma_d(t) \rVert}{\max_i \lVert \sigma_{\hat{d}}(t) \rVert}$	$\mathrm{J8} = \dfrac{\max_f \lVert \sigma_a(t) \rVert}{\max_f \lVert \sigma_{\hat{a}}(t) \rVert}$	$\mathrm{J9} = \dfrac{[\int_0^T f_d(t)\dot{x}_b(t)\,\mathrm{d}t]}{\int_0^T \langle V_0(t)\dot{U}_g(t) \rangle\,\mathrm{d}t}$

*The denominator consists of the corresponding response quantity in the uncontrolled case f = floor number, $1, \ldots, 5$; t = time, $0 \leqslant t \leqslant T$; $\langle \cdot \rangle$ = inner product; $\lVert \cdot \rVert$ = vector magnitude; V_0, V_1 = base and structural shears; x_b = base displacement; d_f = interstorey drift; a_f = floor acceleration; σ_d and σ_a = RMS base displacement and floor acceleration; $\hat{}$ = corresponding response quantity in the uncontrolled case.

Table II. Results for the H_∞ active control.

Earthquake	Case	J1	J2	J3	J4	J5	J6	J7	J8	J9
Newhall	FN	0.68 (−36.2)	0.73 (−30.7)	0.67 (−13.3)	0.74 (−30.1)	0.90 (−45.2)	0.46	0.61	0.71	—
	FP	0.45 (−27.3)	0.52 (−20.2)	0.35 (1.9)	0.55 (−22.2)	0.79 (−49.8)	0.64	0.29	0.38	—
Sylmar	FN	0.59 (−18.8)	0.60 (−19.9)	0.50 (−16.7)	0.60 (−19.9)	0.68 (−15.7)	0.22	0.30	0.34	—
	FP	0.43 (−33.8)	0.44 (−33.2)	0.38 (−22.8)	0.44 (−33.2)	0.48 (−36.6)	0.40	0.26	0.30	—
Rinaldi	FN	0.70 (−27.1)	0.70 (−29.8)	0.75 (−1.3)	0.70 (−29.8)	0.76 (−33.7)	0.29	0.50	0.59	—
	FP	0.49 (−20.9)	0.50 (−21.9)	0.41 (−14.7)	0.50 (−21.9)	0.58 (−20.0)	0.30	0.32	0.34	—
Kobe	FN	0.61 (−34.8)	0.60 (−37.1)	0.57 (−15.0)	0.60 (−37.0)	0.64 (−52.3)	0.47	0.58	0.65	—
	FP	0.52 (−38.0)	0.55 (−35.9)	0.48 (−6.5)	0.57 (−34.2)	0.75 (−58.9)	0.61	0.48	0.56	—
Jiji	FN	0.90 (43.9)	0.90 (44.1)	0.81 (52.6)	0.90 (44.1)	0.90 (37.2)	0.10	0.80	0.78	—
	FP	0.83 (13.2)	0.83 (12.2)	0.81 (43.2)	0.83 (12.2)	0.83 (7.0)	0.22	0.87	0.71	—
Erzinkan	FN	0.61 (−26.7)	0.62 (−27.2)	0.52 (−24.9)	0.62 (−27.2)	0.62 (−32.0)	0.24	0.36	0.41	—
	FP	0.55 (−27.9)	0.56 (−26.0)	0.52 (−3.6)	0.56 (−26.0)	0.68 (−21.5)	0.44	0.31	0.37	—

Percent reductions compared to passive case ($\theta = 0^\circ$) are given inside the brackets.

Table III. Results for the case of maximum friction—passive.

Earthquake	Case	J1	J2	J3	J4	J5	J6	J7	J8	J9
Newhall	Fault-normal	1.06	1.05	0.77	1.05	1.65	0.27	0.63	1.28	0.84
	Fault-parallel	0.62	0.65	0.34	0.71	1.57	0.45	0.17	0.71	0.91
Sylmar	Fault-normal	0.73	0.74	0.60	0.74	0.80	0.18	0.38	0.48	0.77
	Fault-parallel	0.66	0.66	0.50	0.66	0.75	0.24	0.28	0.46	0.84
Rinaldi	Fault-normal	0.96	1.00	0.76	1.00	1.15	0.20	0.52	0.80	0.78
	Fault-parallel	0.62	0.64	0.48	0.64	0.73	0.22	0.30	0.46	0.83
Kobe	Fault-normal	0.93	0.96	0.67	0.96	1.34	0.28	0.62	1.49	0.83
	Fault-parallel	0.84	0.86	0.52	0.86	1.82	0.39	0.45	1.44	0.88
Jiji	Fault-normal	0.63	0.63	0.53	0.63	0.66	0.15	0.42	0.49	0.68
	Fault-parallel	0.73	0.74	0.56	0.74	0.77	0.23	0.43	0.63	0.60
Erzinkan	Fault-normal	0.84	0.85	0.69	0.85	0.92	0.17	0.48	0.59	0.76
	Fault-parallel	0.76	0.76	0.54	0.76	0.86	0.28	0.31	0.54	0.88

uncontrolled case. The floor accelerations are also reduced by 20–59% in a majority of earthquakes when compared to the passive case and 10–52% when compared to the uncontrolled case.

For the case of semiactive control, the SAIVF device located at the isolation level adjusts its position based on the output of the control algorithm (angle, θ). The response of the building when the device is in its closed position ($\theta = 0^\circ$) is given in Table III; the device generates maximum frictional force at all time instants in this position. The results of the semiactive control is presented in Table IV along with the percentage reductions compared to the passive (closed) case ($\theta = 0^\circ$ maximum friction) shown inside the brackets for the peak absolute performance indices, J1–J5. A total of 12 records from six near-fault earthquakes are used in this analytical study. The uncontrolled response quantities are presented in Tables V and VI. The shears are normalized by the total weight of the structure, W (356 000 N), and the accelerations are normalized by acceleration due to gravity, g (9.81 m/s^2). Figure 9 shows the comparison of uncontrolled, passive and semiactive cases for peak values of base shear, base displacement, inter-storey drifts and floor accelerations as a function of maximum foundation acceleration (g). From Figure 9 it is clear that the semiactive control performs better than the passive case in reducing the peak base shear, interstorey drifts and peak floor accelerations for higher ground motion intensities. Figure 10 shows the peak inter-storey drifts (J4) and peak floor accelerations (J5) for the semiactive, passive, and uncontrolled cases for all floors in the case of Newhall (FN, FP) and Kobe (NS, EW) earthquakes. Figure 11 shows the time history responses of the semiactive case for base shear, base acceleration, and the SAIVF device force for the case of Kobe (NS) earthquake. Figure 12 shows the semiactive control and passive force displacement loops for the case of Kobe (NS) earthquake.

The results of the simulation for semiactive control with no stiffness uncertainty (Table IV) shows that both the base shear and structural shear (measured by performance indices J1 and J2, respectively) are reduced by 5–22% when compared to the passive case. These reductions are between 3 and 50% when compared to the uncontrolled case. The magnitude of reductions are comparatively higher for the fault-parallel (FP) components than the fault-normal (FN) components when compared to the uncontrolled case.

Table IV. Results for the semiactive controlled case.

Earthquake	Case	J1	J2	J3	J4	J5	J6	J7	J8	J9
Newhall	FN	0.99 (−6.4)	0.97 (−8.3)	0.74 (−4.2)	0.97 (−8.3)	1.10 (−33.2)	0.28	0.66	0.92	0.79
	FP	0.50 (−19.3)	0.53 (−19.2)	0.35 (3.2)	0.58 (−17.5)	1.38 (−12.0)	0.51	0.25	0.46	0.85
Sylmar	FN	0.67 (−7.7)	0.68 (−8.4)	0.60 (−0.5)	0.68 (−8.4)	0.75 (−7.1)	0.19	0.40	0.46	0.74
	FP	0.61 (−7.0)	0.64 (−2.8)	0.49 (−0.8)	0.64 (−2.8)	0.75 (−0.3)	0.25	0.29	0.38	0.82
Rinaldi	FN	0.92 (−3.6)	0.97 (−2.9)	0.78 (1.6)	0.97 (−2.9)	1.13 (−1.8)	0.21	0.55	0.67	0.72
	FP	0.58 (−6.5)	0.59 (−9.2)	0.49 (1.0)	0.59 (−9.2)	0.69 (−5.9)	0.23	0.31	0.40	0.80
Kobe	FN	0.79 (−15.3)	0.78 (−19.2)	0.65 (−2.5)	0.78 (−19.2)	0.97 (−27.6)	0.32	0.64	0.95	0.77
	FP	0.67 (−20.9)	0.68 (−21.7)	0.55 (7.0)	0.68 (−21.7)	0.94 (−48.5)	0.46	0.48	0.77	0.81
Jiji	FN	0.59 (−5.9)	0.60 (−4.7)	0.52 (−3.1)	0.60 (−4.7)	0.61 (−6.9)	0.15	0.42	0.48	0.66
	FP	0.75 (3.1)	0.76 (3.3)	0.59 (3.8)	0.76 (3.3)	0.80 (3.7)	0.22	0.47	0.62	0.59
Erzinkan	FN	0.80 (−4.1)	0.80 (−5.4)	0.70 (1.2)	0.80 (−5.4)	0.85 (−7.9)	0.18	0.52	0.59	0.73
	FP	0.71 (−5.8)	0.72 (−5.1)	0.58 (7.9)	0.72 (−5.1)	0.80 (−7.7)	0.29	0.34	0.44	0.85

Percent reductions compared to passive case ($\theta = 0^\circ$) are given inside the brackets.

Table V. Uncontrolled response quantities (fault-normal components).

	Newhall	Sylmar	Rinaldi	Kobe	Jiji	Erzinkan
Peak base shear (Norm. by W)	0.224	0.537	0.349	0.241	0.801	0.485
Peak str. shear (Norm. by W)	0.226	0.539	0.352	0.243	0.803	0.487
Peak isolator def. (m)	0.340	0.820	0.530	0.366	1.225	0.742
Peak interstorey Drift (cm)	0.194	0.462	0.302	0.208	0.688	0.417
Peak acc. (g)	0.235	0.543	0.362	0.247	0.807	0.490
RMS disp (m)	0.085	0.309	0.140	0.075	0.285	0.278
RMS acc. (g)	0.057	0.204	0.093	0.050	0.188	0.183

W: weight of the structure; g: acc. due to gravity; m: meters; cm: centimeters.

Table VI. Uncontrolled response quantities (fault-parallel components).

	Newhall	Sylmar	Rinaldi	Kobe	Jiji	Erzinkan
Peak base shear (Norm. by W)	0.213	0.408	0.471	0.183	0.393	0.294
Peak str. shear (Norm. by W)	0.214	0.410	0.472	0.186	0.394	0.294
Peak isolator def. (m)	0.326	0.623	0.719	0.279	0.601	0.449
Peak interst. drift (cm)	0.184	0.351	0.405	0.159	0.338	0.252
Peak acc. (g)	0.217	0.416	0.477	0.193	0.396	0.298
RMS disp (m)	0.122	0.233	0.255	0.075	0.134	0.188
RMS acc. (g)	0.080	0.154	0.168	0.050	0.088	0.124

W: weight of the structure; g: acc. due to gravity; m: meters; cm: centimeters.

The effectiveness of the semiactive control is evident (see Figures 9 and 10) from the results of base displacement (performance index J3 in Table IV) which are reduced by 22–65%, and the interstorey drifts (J4 in Table IV), which are reduced by 20–40% in a majority of earthquakes (Figure 10), when compared to the uncontrolled case. These reductions are achieved without a corresponding increase in either the base or the structural shear. The magnitude of base displacements in the semiactive control case are similar to those achieved in the maximum friction case (performance index J3 in Table III). The inter-storey drifts are reduced (3–20%) in the semiactive control case when compared to the passive friction case. In some cases the passive (closed) case performs better than the active control case (both components of Jiji earthquake), whereas, the semiactive control case consistently performs better than the passive (closed) case.

On–off type semiactive switching algorithms may result in increased base and superstructure accelerations in base isolated buildings. Results of the presented semiactive algorithm (performance index J5) show that contrary to on–off type controllers, the peak base and

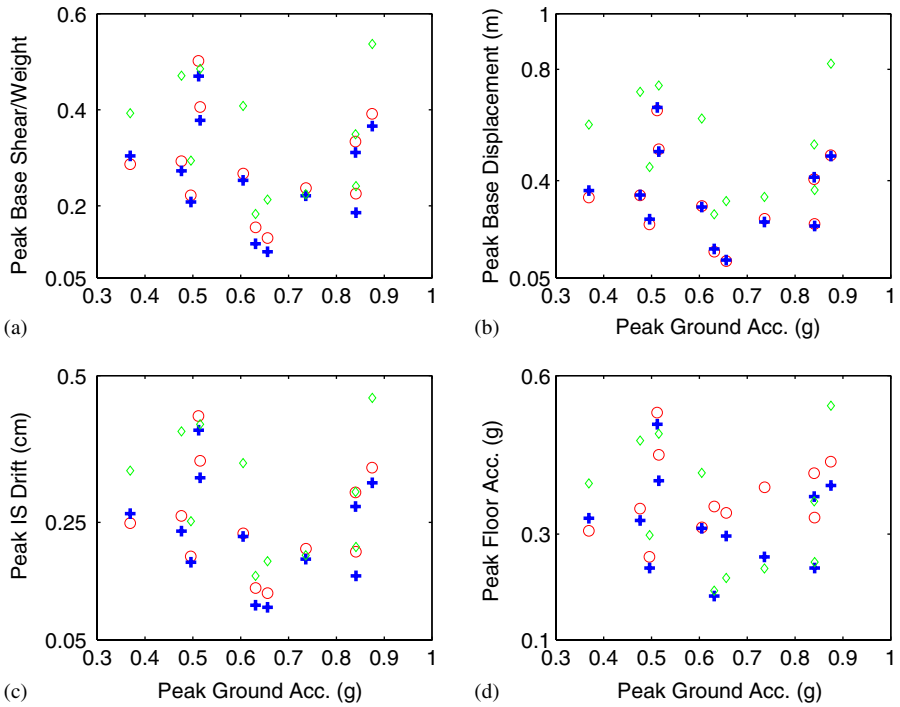

Figure 9. Peak response quantities vs. peak foundation acceleration for: (a) base shear; (b) base displacement; (c) inter-storey drift; and (d) floor acceleration (legend: +: semiactive controlled, o: passive and ◇: uncontrolled).

floor accelerations are reduced in a majority of earthquakes. The reductions in peak floor accelerations for the semiactive control case are between 2 and 50% when compared to the passive case and 3–39% when compared to the uncontrolled case. The results show that the magnitude of peak floor accelerations are lower in the semiactive control case when compared to the passive maximum friction case (Figure 10).

The RMS values of base displacement and floor accelerations (J7 and J8, respectively in Tables III and IV) are also reduced in the semiactive control case and these values are lower in magnitude compared to the passive case. The smooth switching occurs during periods of maximum response resulting in a reduction of the total isolation level force and accelerations as shown in Figures 11 and 12, whereas, in the passive (closed) case the acceleration increases.

7.1. Stiffness uncertainty of ±10%

The performance of both the active and the semiactive control strategies is investigated for the case of stiffness uncertainty of ±10%. The performance of the aforementioned controllers (both active and semiactive) is investigated by means of the resulting performance indices described earlier. Complete results of this robustness simulation study are not presented here due to space limitations. From the results of the study, for the case of active control, the performance of

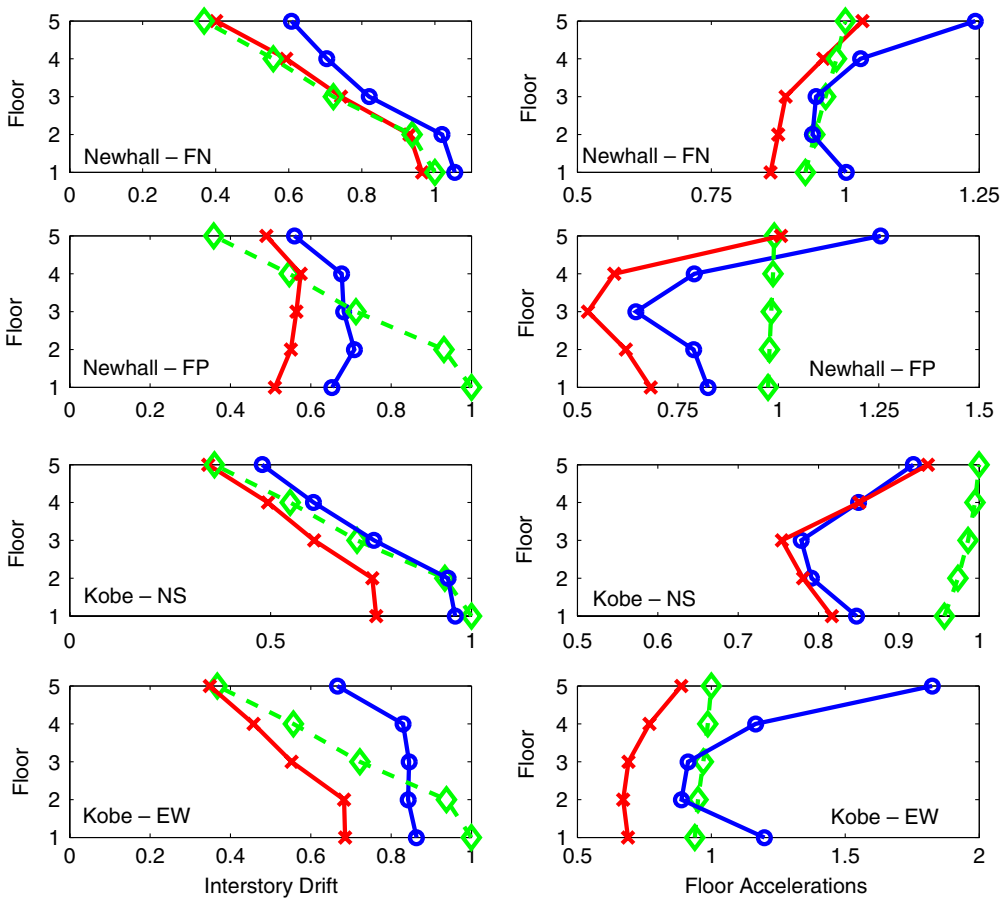

Figure 10. Peak interstorey drifts and floor accelerations normalized by uncontrolled values for a set of near-fault earthquakes in the semiactive case (−x−: semiactive controlled, −o−: passive on and ⋄: uncontrolled).

the controller with stiffness uncertainty of ±10% was found to be comparable to the case with no stiffness uncertainty. Similarly, the results of simulation for semiactive control with ±10% stiffness uncertainty show that the performance of the controller is comparable to the case with no stiffness uncertainty. This clearly indicates the robustness of the developed H_∞ active and semiactive controllers.

8. CONCLUSIONS

Active control based on H_∞ is implemented on the base isolated structure. A new semiactive control algorithm based on H_∞ and frequency-dependent weighting filters are developed

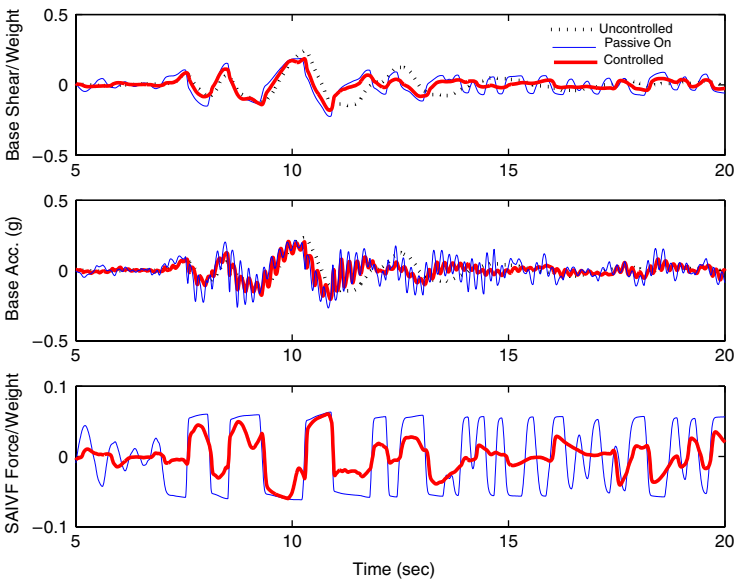

Figure 11. Semiactive control time history results for base shear, base acceleration and SAIVF force subjected to Kobe-NS earthquake.

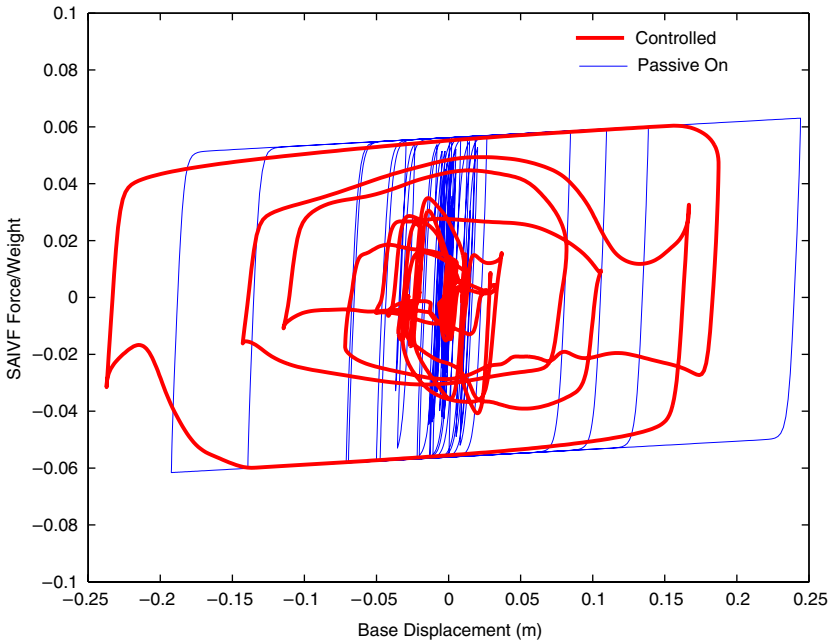

Figure 12. Force–displacement loops for the SAIVF device subjected to Kobe-NS earthquake.

and shown to be effective in reducing the response of base isolated buildings in near-fault earthquakes. A new variable friction device called SAIVF device that is capable of varying the level of friction force smoothly is also introduced. Experimental results are presented to verify the analytical model of the semiactive device. SAIVF device and the control algorithm are shown to be effective in reducing the response of the smart base isolated building in a set of near-fault earthquakes. Passive friction generally leads to increased floor accelerations and interstorey drifts in base isolated buildings. The new active and semiactive controllers are shown to be effective in reducing structural responses such as base displacements and interstorey drifts without increasing either base shear or structural shear and accelerations. Results of the simulation study indicate that the semiactive control strategy is effective for different near-fault earthquakes of varying intensities. The nature of the new semiactive device eliminates the disadvantages associated with some abrupt switching devices. In many cases the passive case performs better than the active control case; however, the semiactive controlled case consistently performs better than the passive case. The results of the simulation study in the presence of stiffness uncertainty show that both the active and semiactive H_∞ controllers are robust and effective in achieving response reductions for smart base isolated buildings during near-fault earthquakes.

ACKNOWLEDGEMENTS

The authors would like to acknowledge the funding for this research provided by National Science Foundation (NSF-CAREER-CMS 9996290).

REFERENCES

1. Spencer BF, Nagarajaiah S. State of the art of structural control. *Journal of Structural Engineering* (ASCE) 2003; **129**(7):845–856.
2. Yang JN, Lin S, Jabbari F. H_∞ based control strategies for civil engineering structures. *Journal of Structural Control* 2004; **10**:205–230.
3. Yang JN, Lin S, Jabbari F. H_2 based control strategies for civil engineering structures. *Journal of Structural Control and Health Monitoring* 2003; **11**(3):223–237.
4. Yang JN, Wu J, Kawashima K, Unjoh S. Hybrid control of seismic-excited bridge structures. *Earthquake Engineering and Structural Dynamics* 1995; **24**(11):1437–1451.
5. Dupont P, Kasturi P, Stokes A. Semiactive control of friction dampers. *Journal of Sound and Vibration* 1997; **202**(2):203–218.
6. Feng MQ. Application of hybrid sliding isolation systems to buildings. *Journal of Engineering Mechanics* 1993; **119**:2090–2108.
7. Fujita *et al*. Semiactive seismic isolation system using controllable friction damper. *Bulletin of Earthquake Resistant Structure Research Center*, vol.27. University of Tokyo; 1994.
8. He WL, Agrawal AK, Yang JN. Novel semiactive friction controller for linear structures against earthquakes. *Journal of Structural Engineering* 2003; **129**(7):941–950.
9. Hirai J, Naruse M, Abiru H. Structural control with variable friction damper for seismic response. In *Proceedings of the Eleventh World Conference on Earthquake Engineering*, Paper No. 1934, Elsevier Science Ltd.: Amsterdam, 1996.
10. Inaudi JA. Modulated homogeneous friction: a semiactive damping strategy. *Earthquake Engineering and Structural Dynamics* 1997; **26**:361–376.
11. Nadathur V, Nagarajaiah S. Wind response control of building with variable stiffness tuned mass damper using empirical mode decomposition and hilbert transform. *Journal of Engineering Mechanics* (ASCE) 2004; **130**(4):451–458.
12. Nagarajaiah S, Mate D. Semi-active control of continuously variable stiffness system. *Proceedings of the 2nd World Conference on Structural Control*, vol. 1, Wiley: New York, 397–405.
13. Nagarajaiah S, Riley MA, Reinhorn AM. Control of sliding-isolated bridge with absolute acceleration feedback. *Journal of Engineering Mechanics* (ASCE) 1993; **119**(11):2317–2332.

14. Narasimhan S, Nagarajaiah S. STFT algorithm for semiactive control of base isolated buildings with variable stiffness isolation systems subjected to near fault earthquakes. *Engineering Structures* 2005; **27**:514–523.
15. Nishitani A, Nitta Y, Ikeda Y. Semiactive structural control based on variable slip-force level dampers. *Journal of Structural Engineering* (ASCE) 2003; **129**(7):933–940.
16. Stammers CW, Sireteanu T. Vibration control of machines by use of semiactive dry friction damping. *Journal of Sound and Vibration* 1998; **209**(4):671–684.
17. Yang JN, Agrawal A. Semiactive hybrid control systems for nonlinear building against near-fault earthquakes. *Journal of Engineering Structure* 2002; **24**(3):271–280.
18. Yang JN, Wu J, Reinhorn A, Riley M. Control of sliding-isolated buildings using sliding-mode control. *Journal of Structural Engineering* (ASCE) 1996; **122**:179–186.
19. Nagarajaiah S, Reinhorn AM, Constantinou MC. Nonlinear dynamic analysis of 3-d-base-isolated structures. *Journal of Structural Engineering* (ASCE) 1991; **117**(7):2035–2054.
20. Narasimhan S, Nagarajaiah S, Johnson EA, Gavin HP. Smart base isolated benchmark building Part I: problem definition. *Journal of Structural Control and Health Monitoring*, Published online November 2005.
21. Yang JN, Li Z, Wu JC, Hsu IR. Control of sliding-isolated buildings using dynamic linearization. *Journal of Engineering Structures* 1994; **16**(6):437–444.
22. Madden GJ, Symans MD, Wongprasert N. Experimental verification of seismic response of building frame with adaptive sliding base isolation system. *Journal of Structural Engineering* (ASCE) 2002; **128**(8):1037–1045.
23. Nagarajaiah S. Fuzzy controller for structures with hybrid isolation system. *Proceedings of the 1st World Conference on Structural Control*, vol. TA2. Los Angeles, CA, 1994; 67–76.
24. Ramallo J, Johnson EA, Spencer B. Smart base isolation systems. *Journal of Engineering Mechanics* (ASCE) 2002; **128**(10):1088–1099.
25. Yoshida K, Yoshida S, Takeda Y. Semi-active control of base isolation using feedforward information of disturbance. *Proceedings of the 2nd World Conference on Structural Control*, vol. 1, Kyoto, Japan, 1999; 377–386.
26. Yoshioka H, Ramallo JC, Spencer BF. Smart base isolation systems employing magnetorheological dampers. *Journal of Engineering Mechanics* (ASCE) 2002; **128**(5):540–551.
27. Nagarajaiah S, Narasimhan S. Smart base isolated benchmark building Part II: phase I sample controllers for linear isolation system: *Journal of Structural Control and Health Monitoring*, Published online November 2005; in print issue 2, 2006.
28. Gavin HP, Alhan C, Natasha O. Fault tolerance of semiactive seismic isolation. *Journal of Structural Engineering* 2003; **129**(7):922–932.
29. Sahasrabudhe S, Nagarajaiah S. Semiactive control of sliding isolated bridges using MR dampers: an experimental and numerical study. *Earthquake Engineering and Structural Dynamics*, Published online on 31 January 2005.
30. Madden G, Wongprasert N, Symans MD. Analytical and numerical study of a smart base isolation system for seismic protection of buildings. *Computer Aided Civil Infrastructure Engineering* 2003; **18**:19–30.
31. Jabbari F, Schmitendorf WE, Yang JN. H_∞ control for seismic excited buildings with acceleration feedback. *Journal of Engineering Mechanics* (ASCE) 1995; **121**(9):994–1002.
32. Kose IE, Schmitendorf WE, Jabbari F, Yang JN. H_∞ active seismic response control using static output feedback. *Journal of Engineering Mechanics* (ASCE) 1996; **122**(7):651–659.
33. Wongprasert N, Symans MD. Experimental evaluation of adaptive elastomeric base-isolated structures using variable-orifice fluid dampers. *Journal of Structural Engineering* (ASCE) 2005; **131**(6):867–877.
34. Yoshida K, Kang S, Kim T. LQG control and H_∞ control of vibration isolation for MDOF systems. *Proceedings of the 1st World Conference on Structural Control*, vol. TA4, Los Angeles, CA, 1994; 43–52.
35. Yang JN, Li Z, Liu SC. Stable controllers for instantaneous optimal control. *Journal of Engineering Mechanics* (ASCE) 1992; **118**(8):1612–1630.
36. Nagarajaiah S. Structural vibration damper with continuously variable stiffness. U.S. Patent 6,098,969, Washington, DC, 2000.
37. Wen YK. Method of random vibration of hysteretic systems. *Journal of Engineering Mechanics* (ASCE) 1976; **102**(2):249–263.
38. Park YJ, Wen YK, Ang AHS. Random vibration of hysteritic systems under bi-directional ground motions. *Earthquake Engineering and Structural Dynamics* 1986; **14**(4):543–557.
39. Francis BA. *A Course in H_∞ Theory*. Springer: Berlin, 1987.
40. Doyle JC, Glover K, Khargonekar PP, Francis BA. State-space solutions to standard H_2 and H_∞ control problems. *IEEE Transactions on Automatic Control* 1989; **34**(8):831–847.
41. Burl BJ. *Linear Optimal Control*. Addison Wesley Longman, Inc.: Reading MA, 1999.
42. Green M, Limebeer DJN. *Linear Robust Control*. Prentice-Hall: Englewood Cliffs, NJ, 1995.
43. Safanov MG, Limebeer DJN. Simplifying the H_∞ theory via loop shifting. *Proceedings of the 27th IEEE Conference on Decision and Control*, Austin, Texas, 1988; 1399–1404.
44. MATLAB. The Math Works, Inc., Natick, MA, 2000.

